NASA TECHNICAL NOTE

NASA TN D-6647
c. 1

NASA TN D-6647

INVESTIGATION OF A MIXED COMPRESSION AXISYMMETRIC INLET AT MACH NUMBER 5.3

by Eldon A. Latham, Norman E. Sorensen, and Donald B. Smeltzer

Ames Research Center
Moffett Field, Calif. 94035

NATIONAL AERONAUTICS AND SPACE ADMINISTRATION • WASHINGTON, D. C. • JANUARY 1972

1. Report No. NASA TN D-6647	2. Government Accession No.	3. Recipient's Catalog No.

4. Title and Subtitle

INVESTIGATION OF A MIXED COMPRESSION AXISYMMETRIC INLET AT MACH NUMBER 5.3

5. Report Date: January 1972

6. Performing Organization Code:

7. Author(s)

Eldon A. Latham, Norman E. Sorensen, and Donald B. Smeltzer

8. Performing Organization Report No.: A-4160

9. Performing Organization Name and Address

NASA–Ames Research Center
Moffett Field, Calif., 94035

10. Work Unit No.: 764-74-01-00-21

11. Contract or Grant No.:

12. Sponsoring Agency Name and Address

National Aeronautics and Space Administration
Washington, D. C., 20546

13. Type of Report and Period Covered: Technical Note

14. Sponsoring Agency Code:

15. Supplementary Notes

16. Abstract

The hypersonic diffuser portion of an uncooled high performance mixed compression, axisymmetric inlet suitable for subsonic burning engines has been designed and tested. Performance of a model with a 25.4-cm capture diameter was measured in a wind tunnel and the results were compared with theoretical predictions calculated by a comprehensive computer program. All tests were conducted at a Mach number of 5.3 at a total temperature of 667° K and a total pressure of 11.57 atm. The angle of attack ranged from 0° to ±3°. Performance at angle of attack remained high. Reasonably high performance in the throat (maximum throat pitot-pressure recovery of 77 percent and an average value of 58 percent) was obtained at 0° angle of attack with relatively large amounts of boundary-layer bleed (11 to 22 percent of the capture mass flow).

The computer program used in the design of this inlet is considered marginally adequate for predicting hypersonic inlet flow fields. Although the program as it now exists is very useful, an improved computer program that more accurately predicts the boundary layer and the shock-wave—boundary-layer interaction, and accounts for boundary-layer bleed should be developed for reliably predicting hypersonic inlet flow fields.

17. Key Words (Suggested by Author(s))	18. Distribution Statement
Inlet Hypersonic Axisymmetric Boundary layer Inlet design Propulsion system	Unclassified -- Unlimited

19. Security Classif. (of this report)	20. Security Classif. (of this page)	21. No. of Pages	22. Price*
Unclassified	Unclassified	35	$3.00

*For sale by the National Technical Information Service, Springfield, Virginia 22151

SYMBOLS

A_c	capture area
A_{th}	throat area
D	capture diameter
h	local rake tube height
M	Mach number
m	mass flow
p	static pressure
p_p	pitot pressure
p_t	total pressure
R	capture radius
r	local radius
T_t	total temperature
x	axial distance measured from the tip of the centerbody
x_c	axial distance measured from the cowl lip
α	inlet angle of attack
δ	boundary-layer height
η_{KE}	kinetic energy efficiency
$(\bar{\ })$	average

Subscripts

bl	bleed	th	throat
c	cowl	l	local
cb	centerbody	∞	free stream

INVESTIGATION OF A MIXED COMPRESSION AXISYMMETRIC INLET AT MACH NUMBER 5.3

Eldon A. Latham, Norman E. Sorensen, and Donald B. Smeltzer

Ames Research Center

SUMMARY

A hypersonic, axisymmetric, mixed-compression inlet designed for Mach number 5.3 has been tested. The hypersonic diffuser was designed for high theoretical performance suitable for subsonic burning engines. Performance of only the hypersonic diffuser up to the throat of a 25.4-cm capture diameter, uncooled model was measured in the Ames 3.5-Foot Hypersonic Wind Tunnel. All tests were conducted at Mach number 5.3 at a total temperature of 667° K and a free-stream total pressure of 11.57 atm. The Reynolds number was 7.77×10^5/m, and the angle of attack ranged from 0° to ±3°. The wind-tunnel results were compared with predictions calculated by a comprehensive computer program that accounted for the boundary layer as well as the inviscid flow field.

Although relatively high performance was obtained at 0° angle of attack (maximum throat pitot-pressure recovery of 77 percent and an average value of 58 percent), the inlet could not be operated at the design contraction ratio. A number of boundary-layer bleed patterns were investigated in an attempt to obtain maximum performance, but relatively large amounts of boundary-layer removal (11 to 22 percent capture mass flow) were required to approach the design contraction ratio. Performance at all test angles of attack remained high.

Two computer programs were used to develop the inlet contours. An inviscid program, which used the method of characteristics, was used for the preliminary design and an inviscid-viscous program, which accounted for the boundary layer, was used to establish the final contours. Although the inviscid-viscous program as it now exists is very useful in the development of inlet contours, it is considered marginally adequate for predicting inlet flow fields. An improved computer program that more accurately predicts boundary-layer parameters and shock-wave—boundary-layer interactions, and accounts for boundary-layer bleed should be developed for reliably predicting hypersonic inlet flow fields.

INTRODUCTION

Hypersonic vehicles designed to cruise in the Mach number 6.0 regime require high performance propulsion systems with subsonic burning ramjet or turboramjet engines (refs. 1 and 2). To minimize terminal shock losses the inlets of such propulsion systems must compress the airflow entering the hypersonic diffuser to a relatively low supersonic speed in the throat. One likely inlet candidate employs a short (lightweight), mixed-compression, axisymmetric, hypersonic diffuser with high performance capabilities based on the results of a computer program. Properly compressing the entering airflow in a short length, without causing separation of the boundary layer

in the hypersonic diffuser, creates a difficult design problem because of shock waves impinging on the boundary layer in high adverse pressure gradients. The problem was attacked by designing an inlet system with the aid of a computer program, and comparing the analytical results with experimental data. The computer program utilized the method of characteristics and boundary-layer theories to calculate the hypersonic flow-field characteristics. In the experimental portion of the program, a model of a relatively short hypersonic diffuser designed with the aid of the computer program was tested in a wind tunnel. The objective of the experimental program was to establish the adequacy of the computer program for designing hypersonic diffuser contours suitable for subsonic burning engines and for predicting the inlet performance.

The hypersonic diffuser was designed for Mach number 5.3, which is approximately the Mach number under the wing of a Mach number 6.0 cruise vehicle. The model having a capture diameter of 25.4 cm was tested in the Ames Research Center 3.5-Foot Hypersonic Wind Tunnel. All tests were conducted at Mach number 5.3 with a free-stream total temperature of 677° K, a free-stream total pressure of 11.57 atm, a Reynolds number of approximately 7.77×10^5/m, and an angle-of-attack range from 0° to ±3.0°.

MODEL

The axisymmetric hypersonic diffuser model had a translating centerbody and was designed for shock on lip at Mach number 5.3. The model, consisting of only the hypersonic diffuser, was uncooled and had a capture diameter of 25.4 cm. Figure 1 is a photograph of the model mounted in the Ames 3.5-Foot Hypersonic Wind Tunnel; the model geometry is shown in figure 2(a). The inlet coordinates are listed in table 1. Boundary-layer control was provided by porous bleed regions on the centerbody and cowl surfaces in the vicinity of the throat (fig. 2(b)). The bleed regions consist of 1.5875-mm-diameter holes drilled normal to the model centerline, creating areas with 40-percent porosity. Selected bleed holds were filled with ceramic filler material to obtain various porous patterns. The bleed-flow plenum exit areas were set by manually positioning threaded control rings for each run. The bleed patterns tested are shown in figure 3. Before bleed pattern B was tested, the model centerbody contour (aft of the throat station, $x/R = 4.735$) was modified to relieve a small amount of blockage. This contour modification is shown in figure 3(b).

INSTRUMENTATION

Instrumentation consisted of static-pressure orifices, throat total-pressure rakes, a boundary-layer total-pressure rake, and bleed plenum total-pressure tubes as indicated in figure 2(b). Static-pressure orifices were located in the pitch plane of the model along the centerbody and cowl surfaces. Additional static orifices were located at 90° intervals around the duct on both the cowl and centerbody in the throat region. The throat total pressure was measured with two seven-tube rakes, each with different tube spacing for complete coverage of the throat region. During wind-tunnel operations only one rake was installed on the model at any time to prevent possible interference. A run with each rake was required to obtain a complete profile. The boundary-layer rake consisted of eight tubes and was located on the forward portion of the centerbody (fig. 2(b)). A sketch of all rakes is shown in figure 4. Bleed-flow rates through the cowl

and centerbody surfaces were calculated from the known choked exit areas and measured plenum chamber total pressures.

DESIGN PROCEDURE

Two computer programs were used to calculate the inlet flow field. One was an inviscid program that did not account for the presence of the boundary layer and employed only the method of characteristics (ref. 3). The other was an inviscid-viscous program that simultaneously combined boundary-layer solutions with the method of characteristics (ref. 4). Supersonic mixed-compression inlets for Mach numbers of at least 3.5 were successfully designed solely by the inviscid program (ref. 5). The amount of boundary-layer bleed required to prevent separation of the boundary layer in these inlets (5-10 percent of the capture mass flow) compensated very closely for the effective contour displacement that resulted from the presence of the boundary layer. However, for the present hypersonic inlet design, this relatively simple approach was believed to be inadequate because of the relatively thick boundary layers anticipated in the throat. Nevertheless, the inviscid program was used to develop preliminary contours because it is much quicker and easier to use than the viscous program. Once the preliminary design was established the final contours were determined with the aid of the viscous program.

To account for the presence of the boundary layer, the viscous program (as outlined in ref. 4) used the local similarity method to solve numerically the classical laminar boundary-layer equations. The turbulent boundary-layer solution employed is a first-order integral parameter solution in which a power law velocity profile and the skin-friction law of Sivells and Payne were used with a reference enthalpy procedure to account for the effects of compressibility. For the development of the boundary layer in the transition region between laminar and turbulent flow, the program used a modified form of the skin-friction law initially proposed by Persh (ref. 6). Constants used in the relationship expressing the local skin-friction coefficient as a function of the turbulent skin-friction coefficient and the Reynolds number based on the momentum thickness are based on experimental results for flat plates and cones. In addition, empirical incompressible relationships were combined with a reference enthalpy method and a compressibility transformation to determine the boundary-layer-momentum thickness distribution in the transition region.

The accuracy of the laminar boundary-layer predictions is considered adequate when edge vorticity and normal pressure gradient effects are small. The turbulent boundary-layer predictions, however, are questionable because of the crudeness of the transitional and turbulent flow models employed, and the requirements imposed by inlet design, such as severe adverse pressure gradients. For this inlet design the start of transition was selected to allow fully turbulent flow at $x_c/R = 0.47$ and $x/R = 2.80$ for the cowl and centerbody, respectively. The locations for the start of fully developed turbulent flow were based on experimental data. Sublimation studies conducted on this model indicated that the centerbody boundary layer was fully turbulent at approximately $x/R = 2.7$.

The design criteria for the hypersonic diffuser did not allow the sudden pressure rises across the shock waves impinging on the cowl and centerbody to exceed the rise for incipient separation (ref. 7). Without violating the separation criteria, the inlet was designed to achieve a theoretical pressure recovery of about 93 percent in the inviscid core flow at the throat with the shortest

practical diffuser length. The theoretical Mach number in the inviscid portion of the flow in the throat was about 1.25. Because the model was uncooled, the theoretical solutions for the boundary layer were calculated in the program with assumed adiabatic wall conditions at an average wall temperature of 444° K (the program cannot account for the actual varying wall temperature, but other average wall temperatures were assumed with no significant change in the boundary layer) and actual wind-tunnel conditions of 667° K total temperature, 11.47 atm total pressure, and a free-stream Mach number of 5.3.

TEST PROCEDURE

All tests were conducted in the Ames Research Center 3.5-Foot Hypersonic Wind Tunnel at $M = 5.3$, $p_{t_\infty} = 11.57$ atm and $T_{t_\infty} = 667°$ K. Data were obtained at 0° angle of attack for no bleed and bleed pattern A, and at 0°, ±1.5°, and ±3.0° angle of attack for bleed pattern B. To minimize heating effects and erosion of the model surfaces caused by dust from the tunnel storage heater, a hydraulically actuated "quick-insert" mechanism was used to insert the model into the airstream once tunnel test conditions had been established. The inlet was inserted into the tunnel with the centerbody extended to a starting contraction ratio of approximately $A_c/A_{th} = 1.4$. The centerbody was then retracted and data were recorded for a series of contraction ratios up to unstart. This procedure maximized the amount of data that could be recorded during the limited running time of each "blow down" of the wind tunnel, approximately 2 min.

PRECISION OF DATA

The model angle of attack was positioned to within ±0.1°; however, stream angle corrections were not included because of the lack of calibration data. The stream angle error is estimated to be less than 0.3°. The estimated accuracy of the remaining measured quantities is as follows:

Parameter	Uncertainty
p_t/p_{t_∞}, p_p/p_t	±0.007
m_{bl}/m_∞	±0.007
p/p_∞	±1.33
M_∞	±0.05
M_Z	±0.02
h	±0.05 mm
T_t	±16.7° K

RESULTS AND DISCUSSION

The results of the investigation are presented in figures 5 through 14 (table 2 is an index to the figures). The performance of the hypersonic diffuser is illustrated quantitatively by pressure distributions plotted along the cowl and centerbody and by plots of pitot pressure and local Mach number profiles in the throat.

Although the model was designed to operate without boundary-layer bleed, flow separation occurred just upstream of the throat on the centerbody so that bleed was required to attain even moderate contraction ratios. Several bleed configurations were tested to achieve the best possible contraction ratio. Although the maximum attainable geometric contraction ratio increased significantly with increasing boundary-layer bleed, the aerodynamic contraction (due to the large amount of flow being removed through the bleed system) increased only slightly, improving inlet performance a relatively small amount. (See fig. 8.)

Each bleed region on the centerbody and on the cowl is connected to a single plenum chamber. Large pressure gradients across such bleed regions make it necessary to maintain sonic flow through the bleed holes to prevent recirculation of the duct flow from high to low pressure areas. If individual compartments had been available for regions of different pressure levels, the bleed flow for each region could have been controlled and optimized independently; this was not possible with the existing bleed system. Further, it is probable that this "choked bleed hole" condition required more boundary-layer bleed than would have been necessary otherwise. Consequently, the bleed configurations tested are not considered optimum.

Performance at Zero Angle of Attack

Static-pressure distribution– Figure 5 compares the surface static-pressure distributions on both the cowl and centerbody of the model in the region of the throat with no bleed and with bleed patterns A and B (see fig. 3). In each case, data are presented for the maximum attainable contraction ratio just before the inlet unstarted. Without bleed, relatively little compression was possible ($(p/p_\infty)_{th} \cong$ 50-60). Wind-tunnel observations of schlieren and pitot-pressure data indicated flow separation on the centerbody in the throat region that limited the maximum contraction ratio to 8.84. The maximum attainable contraction ratio was increased to 13.8 ($(p/p_\infty)_{th} \cong$ 120-130) and 18.2 ($(p/p_\infty)_{th} \cong$ 160) with bleed rates of 11 and 22 percent of the capture mass flows, respectively. Although the theoretical maximum contraction ratio was 22, increasing the bleed rate further was considered impractical.

Figure 6 compares the static-pressure distributions from figure 5 for contraction ratios of 13.8 and 18.2 with the predicted values. Note that the theory does not include the effects of boundary-layer bleed. The inlet geometry and theoretical shock-wave locations are indicated schematically on each figure. In figure 6(a) at a contraction ratio of 13.8, the model surface static pressures are greater than predicted, partly, as will be shown, because of the thicker than anticipated boundary layer which effectively increases the contraction ratio. In figure 6(b) at a contraction ratio of 18.2 a similar effect can be seen except that at the throat so much flow is being removed that the compression cannot increase as much as predicted by theory. The figures show that the theory and data follow the same trends but the pressure levels do not always agree closely.

Figure 7 shows the increase in static pressure as the inlet contraction ratio increases to a maximum for bleed pattern B. The pressure along the centerbody increases smoothly all the way to the throat for contraction ratios of 15.5 and 17.2. For contraction ratios of 17.8 and 18.2 the sudden rise in compression at $x/R = 4.6$ indicates possible local flow separation[1] with almost immediate reattachment. This pressure rise can also be seen in figures 5 and 6(b). The pressures on the cowl increase smoothly through the first shock impingement region and then decrease. It should be noted that expansion as well as compression processes may occur in an inlet flow field as a result of the diffuser contours. At the design contraction ratio the contours provide for continual flow compression, but off design the surfaces can introduce expansions that propagate across the flow field. The decrease in pressure at off-design contraction ratios for this inlet is associated with the flow expansion that originates upstream on the curved centerbody surface and propagates across the stream to the cowl surface. This region of decreased pressure nearly disappears as the contraction ratio approaches the design value. For both the cowl and centerbody the bleed flow rate increases with increased contraction ratio as a result of the higher pressure over the bleed regions.

Throat total pressure and Mach number profiles– Although problems with compression can be identified with careful analysis of the diffuser surface-pressure distributions, the flow properties in the throat are important because they indicate the performance that can be obtained at the engine face. The throat pitot pressure and corresponding Mach number profiles for the three configurations under consideration (at the maximum contraction ratio for each) are shown in figure 8.

Full-span throat measurements are available only for the bleed pattern B configuration. The throat height for each configuration is shown on the figure. Only the local surface static pressure measured on the centerbody and the rake pitot pressure are used to calculate Mach number. Theoretical pitot pressure and Mach number profiles are not included in figure 8 since the computer program could not account for boundary-layer bleed and the comparison was not considered valid. However, the theoretical boundary-layer heights at contraction ratios of 13.81 and 18.20 are indicated for reference. For these flow fields there is some uncertainty in determining the experimental boundary-layer heights because of possible nonuniformities in the inviscid flow field due to the influence of the boundary layer and the large amount of bleed flow. However, according to the usual definition of boundary-layer height (i.e., height where pitot pressure becomes nearly constant), these plots show that the experimental boundary layer for the cowl is much thicker than that predicted by theory even though large amounts of flow were removed by the boundary-layer bleed system. The experimental boundary layer for the centerbody is approximately the same thickness as that predicted by theory; however, this may be fortuitous because of the large bleed flow.

The performance for a complete inlet system with this hypersonic diffuser can be estimated by integrating the pitot-pressure profile and assuming a subsonic diffuser loss of 5-percent total-pressure recovery. At $A_c/A_{th} = 18.2$ (bleed pattern B), a pressure recovery of 53 percent ($\eta_{KE} = 96$ percent) might be expected at the engine face; at $A_c/A_{th} = 13.8$ (bleed pattern A), 46 percent ($\eta_{KE} = 95$ percent) might be expected. Although these values would be higher than the required pressure recovery for the cruise vehicles described in reference 1 (37 percent recovery with

[1] A sudden rise in pressure that cannot be explained by strong shock-wave impingement or by a sudden theoretical pressure rise is believed to indicate flow separation.

no bleed), it is evident that the higher recoveries obtained in the present tests entail high bleed-drag penalties. Perhaps lower recoveries with less bleed would be closer to optimum.

In figure 9 the throat pitot-pressure profiles for different inlet contraction ratios correspond to the surface static-pressure distributions in figure 7 (except for $A_c/A_{th} = 15.87$ which was included to show the profile development) and are for bleed pattern B only. At each contraction ratio, the boundary-layer thickness on each surface appears to remain about the same, nearly causing the inviscid core flow to disappear at $A_c/A_{th} = 18.2$. Over this range most of the increases in compression occurred before a contraction ratio of 17.2 was reached. Practically no change occurred thereafter, since as discussed, the increasing rate of bleed flow reduces the effective contraction ratio.

Centerbody boundary-layer profiles– The pitot pressure and Mach number profiles of the centerbody boundary layer at model station $x/R = 4.2$ are shown in figure 10 along with theoretical predictions. The profiles are the same for all contraction ratios and bleed configurations since this station is forward of the first shock impingement and the bleed regions. At this model station, the actual boundary-layer height is considerably less than predicted by theory; at the throat, on the other hand, theory underpredicts the boundary-layer height. The computer program appears unable to predict the boundary layer accurately on a compression surface even in the absence of shock impingement.

Performance at Angle of Attack

Adequate performance at angle of attack is important to maintain engine thrust while an aircraft is being maneuvered. In addition, the performance at angle of attack indicates the inlet tolerance to unstart caused by sudden external flow changes, such as gusts. Data at angle of attack are available only for bleed pattern B.

Static-pressure distributions– Cowl and centerbody surface static-pressure distributions at $\alpha = 0°$ and $\pm 1.5°$ are compared in figure 11(a), and at $\alpha = 0°$ and $\pm 3.0°$ in figure 11(b). The data in each figure are for the maximum contraction ratio attainable for the angle-of-attack range under consideration. The compression is greater on the windward side of the model probably because of the greater effective cone angle. Pressure increases are relatively smooth at all angles tested until the expansion regions (previously noted on the cowl for $\alpha = 0°$) are encountered. The contraction ratio at which separation appears on the centerbody has not yet been reached (see fig. 7). Also, as expected, the compression level at $\alpha = \pm 3.0°$ is less than that for $\alpha = \pm 1.5°$ because of the lower contraction ratio.

Throat total pressure and Mach number profiles– Pitot pressure and corresponding Mach number profiles are shown for $\alpha = 0°$ and $\pm 1.5°$ in figure 12(a), and $\alpha = 0°$ and $\pm 3.0°$ in figure 12(b). The contraction ratios for each of these ranges correspond to those for the static-pressure distributions plotted in figures 11(a) and 11(b). As would be expected, the pitot pressures are greater and the Mach number less for $\alpha = \pm 1.5°$ than for $\alpha = \pm 3.0°$ because of the increased contraction ratio at $\alpha = \pm 1.5°$. The difference between contraction ratio in figures 12(a) and 12(b) accounts for the changes in profile shapes. However, relatively little change occurs in the profiles as the angle of attack is varied at a constant contraction ratio. To provide some unstart tolerance to sudden changes in angle of attack, the reduced contraction ratio ($A_c/A_{th} = 17.2$),

which allows the inlet to pitch to $\alpha = \pm 1.5°$, entails a performance penalty of less than 0.5 percent in average p_p/p_{t_∞} at $\alpha = 0°$. For a 3.0° tolerance, 5.3-percent reduction in average p_p/p_{t_∞} at $\alpha = 0°$ results.

Centerbody boundary-layer profiles– The pitot and Mach number profiles of the centerbody boundary layer at model station x/R = 4.2 for $\alpha = 0°$, ±1.5°, and -3.0° are shown in figure 13. Data for $\alpha = 3.0°$ were not obtained.

Data show the influence at this station of angle of attack on the centerbody boundary layer forward of any disturbances caused by shock impingement or boundary-layer bleed. (The data for $\alpha = 0°$ are compared with theory in fig. 10). As the angle of attack increases from $\alpha = -3.0°$ to +1.5°, the pitot pressure level increases with reduction in the effective cone angle, but the boundary-layer thickness remains essentially the same.

Schlieren photographs– Figure 14(a) is a schlieren photograph of the inlet centerbody and cowl at $\alpha = 0°$ and with the geometry for maximum contraction ratio. The centerbody bow shock wave lies just outside the cowl lip, indicating little flow spillage. Figure 14(b) shows the inlet pitched to $\alpha = -3.0°$ with the bow shock wave impinging far inside the cowl lip, indicating that the inlet can tolerate the internal shock-wave impingement on the cowl without unstarting.

CONCLUDING REMARKS

The theoretical performance potential of the design was never achieved. Although the diffuser was designed to operate with no bleed, flow separation just upstream of the throat on the centerbody required boundary-layer bleed before any significant performance could be achieved. Relatively large amounts of bleed on both the cowl and centerbody were necessary to approach the design contraction ratio of 22. A maximum pitot-pressure recovery of 77 percent at the inlet throat was achieved with a boundary-layer bleed flow of approximately 22 percent of the capture mass flow. The estimated engine-face pressure recovery based on this value is 53 percent. However, the high bleed associated with this recovery entails a high drag penalty. Perhaps a lower recovery with less bleed would be closer to optimum. The inlet can operate at 0° angle of attack with a contraction ratio that allows an angle-of-attack range of ±1.5° without unstarting with less than a 0.5-percent pressure recovery loss from that at the maximum attainable contraction ratio.

Although the inviscid-viscous program as it now exists is very useful in the development of inlet contours, the inlet flow-field predictions are considered marginally adequate. The thicker than anticipated throat boundary layers did not allow full contraction of the flow in the inlet, and the predicted performance was not achieved. To predict hypersonic inlet flow fields reliably, an improved program is needed that more accurately predicts the boundary layer and shock-wave — boundary-layer interactions, and accounts for boundary-layer bleed.

Ames Research Center
National Aeronautics and Space Administration
Moffett Field, Calif., 94035, Sept. 22, 1971

REFERENCES

1. Gregory, Thomas J.; Peterson, Richard H.; and Wyss, John A.: Performance Trade-offs and Research Problems for Hypersonic Transports. AIAA Paper 64–605, 1964.

2. Sorensen, Norman E.; Morris, Shelby J.; and Pfyl, Frank A.: A Study of Hypersonic Inlet Technology. NASA SP–148, 1967, pp. 283-297.

3. Sorensen, Virginia L.: Computer Program for Calculating Flow Fields in Supersonic Inlets. NASA TN D–2897, 1965.

4. Maslowe, S. A.; and Benson, John L.: Computer Program for the Design and Analysis of Hypersonic Inlets. NASA CR 77749, 1964.

5. Sorensen, Norman E.; Latham, Eldon A.; and Morris, Shelby J.: Prediction of Supersonic and Hypersonic Inlet Flow Fields. NASA SP–228, 1969, pp. 583-595.

6. Maslowe, S. A.; and Benson, J. L.: A Procedure for Computing Transitional Boundary-Layer Parameters in Compressible Flows. Lockheed Report 20405, Jan. 1967.

7. Kuehn, Donald M.: Experimental Investigation of the Pressure Rise Required for the Incipient Separation of Turbulent Boundary Layers in Two-Dimensional Supersonic Flow. NASA MEMO 1–21–59A, 1959.

TABLE 1.– INLET COORDINATES

Centerbody		Cowl	
x/R	r/R	x_c/R	r/R
0	0	0	1.0000
Straight taper		Straight taper	
2.5000	0.4408	0.1700	1.0090
2.6000	.4588	.2400	1.0124
2.7000	.4774	.3200	1.0156
2.8000	.4966	.4000	1.0184
2.9000	.5166	.5000	1.0208
3.0000	.5374	.6000	1.0226
3.1000	.5588	.7200	1.0232
3.2000	.5808	.7700	1.0222
3.3000	.6040	.8200	1.0188
3.4000	.6272	.8700	1.0132
3.5000	.6512	.9350	1.0030
3.6000	.6758	Straight taper	
3.7000	.7014	1.0100	.9888
3.8000	.7274	1.0400	.9838
3.9000	.7542	1.0550	.9822
4.0000	.7818	Straight taper	
4.1000	.8098	1.3200	.9636
4.2300	.8480		
Straight taper			
4.4850	.9230		
4.5500	.9406		
4.6000	.9524		
4.6500	.9596		
4.6650	.9604		
4.7000	.9602		
4.7200	.9600		
4.7350	.9588		
4.7500	.9574		
5.0000	.9216		

TABLE 2.– INDEX TO FIGURES

Figure	
1	Model photograph
2(a)–2(b)	Sketches of model
3(a)–3(b)	Bleed configurations
4	Rake detail
5	Static-pressure distributions at maximum contraction ratio
6(a)–6(b)	Comparison of data with theoretical static-pressure distribution
7	Static-pressure distributions at various contraction ratios
8	Throat pitot pressure and Mach number profiles
9	Throat pitot-pressure profiles at various contraction ratios
10	Centerbody boundary-layer pitot pressure and Mach number profiles
11(a)–11(b)	Static-pressure distributions at angle of attack
12(a)–12(b)	Throat pitot pressure and Mach number profiles at angle of attack
13	Centerbody boundary-layer pitot pressure and Mach number profiles at angle of attack
14(a)–14(b)	Schlieren photographs

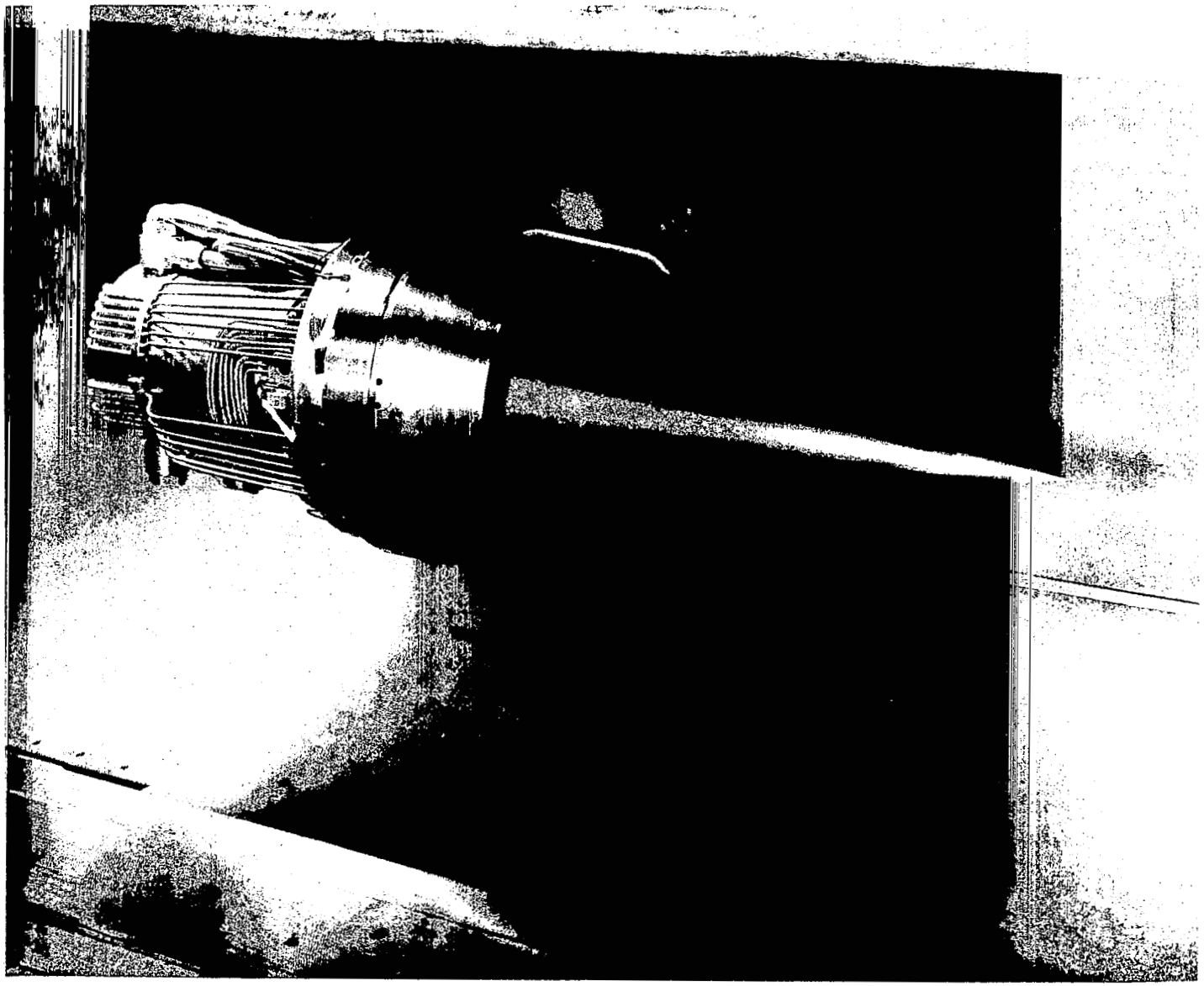

Figure 1.- Model mounted in Ames 3.5-Foot Hypersonic Wind Tunnel.

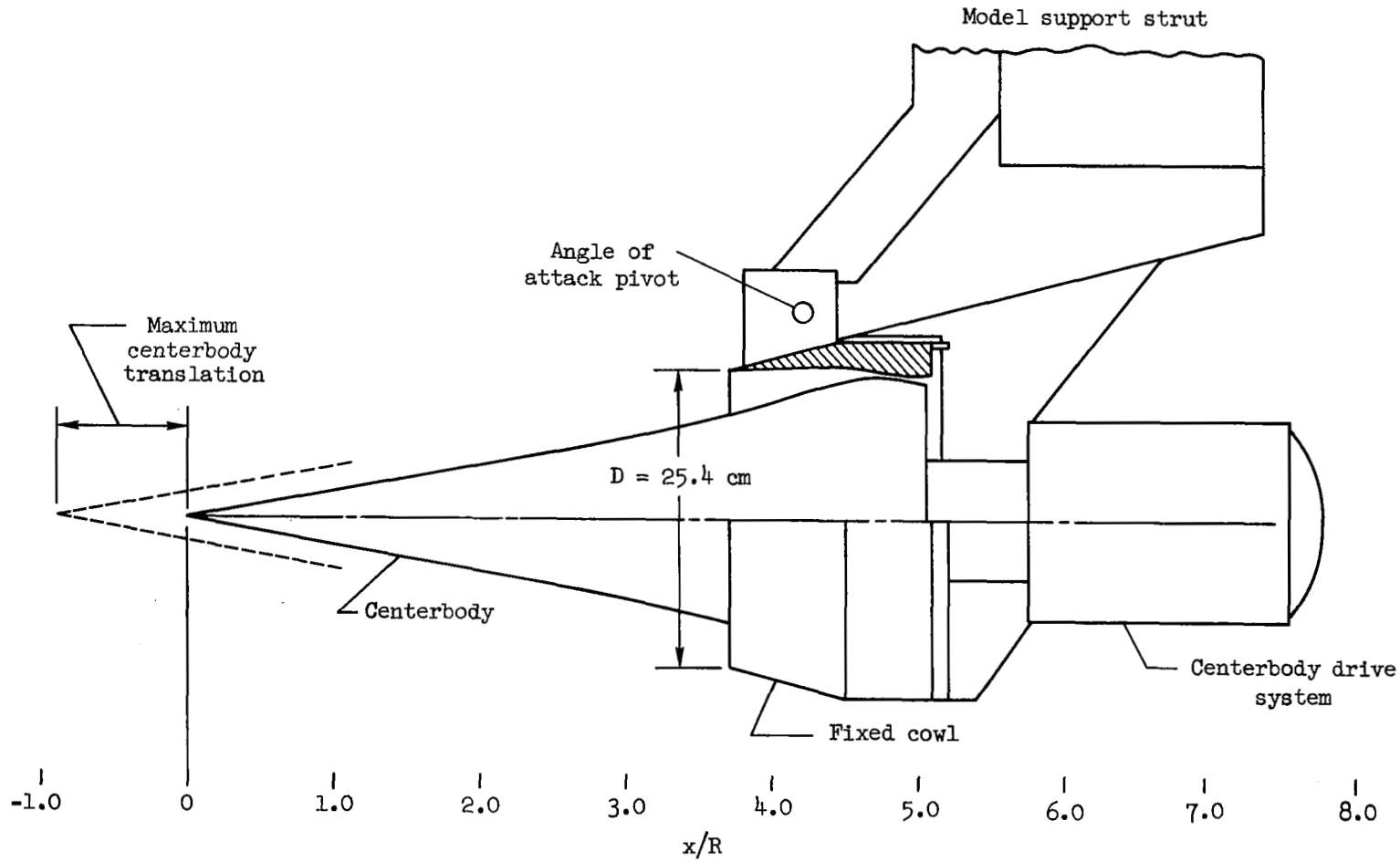

(a) Overall model

Figure 2.- Model geometry.

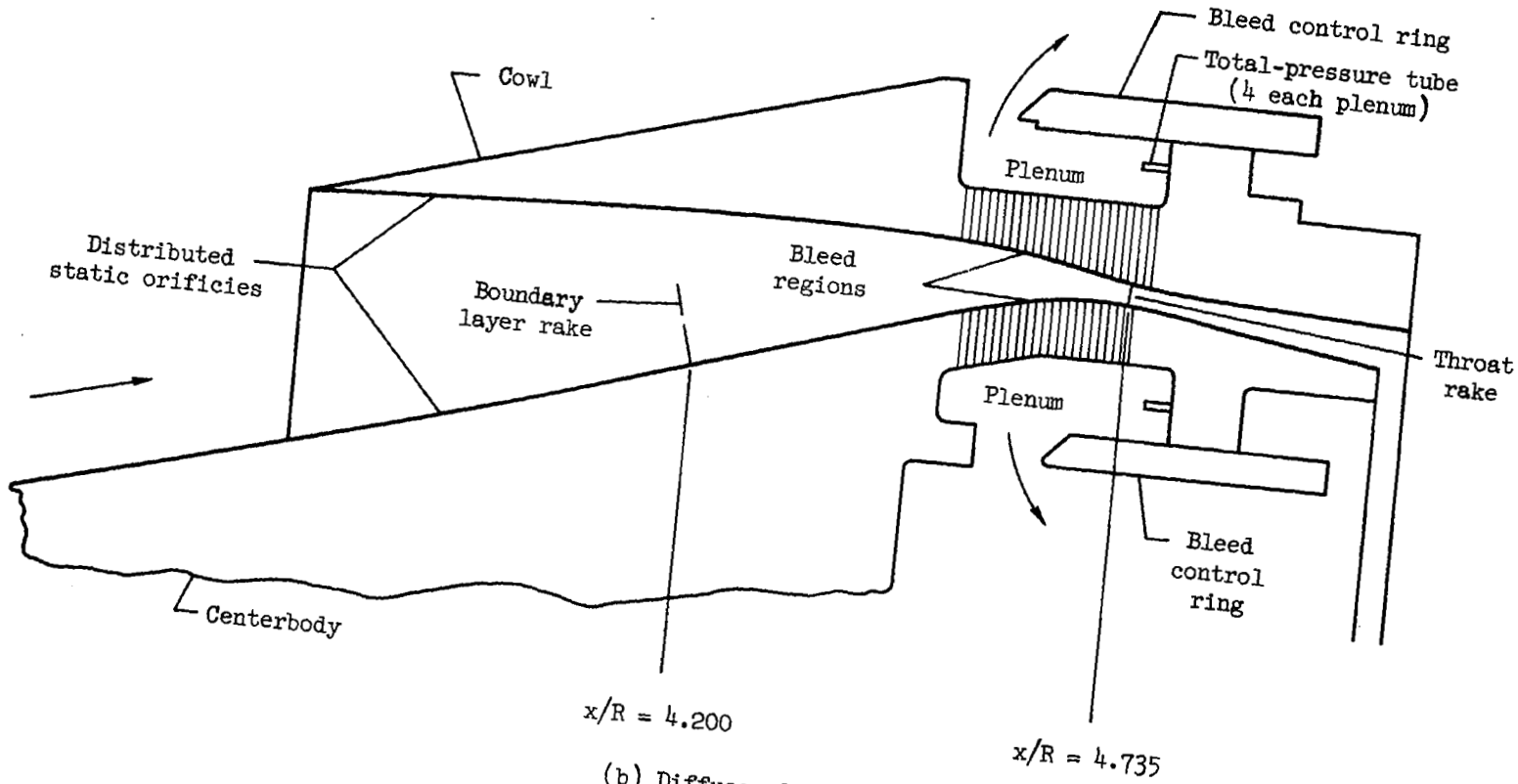

(b) Diffuser detail

Figure 2.- Concluded.

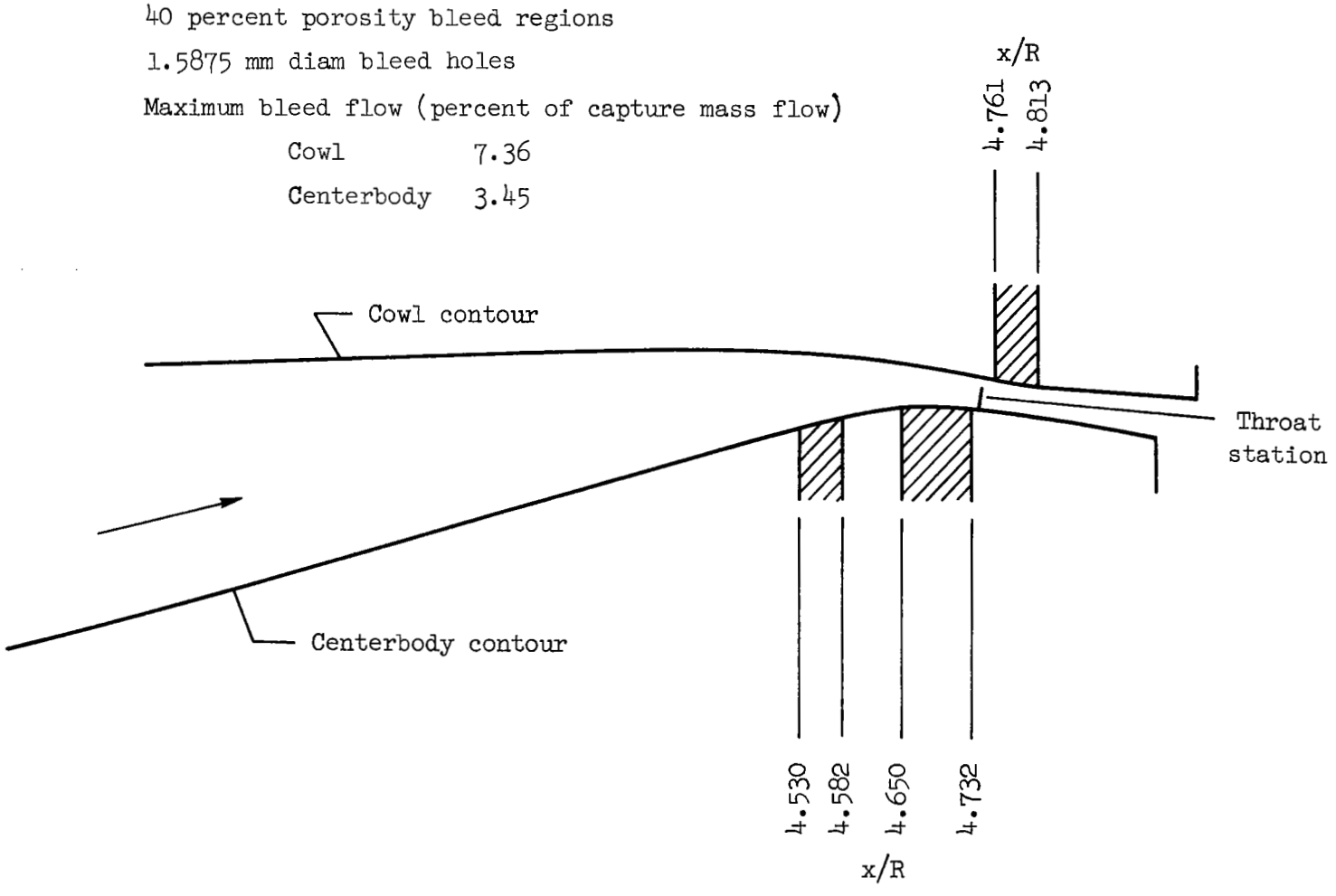

(a) Bleed pattern A

Figure 3.- Bleed configuration.

40 percent porostiy bleed regions

1.5875 mm diam bleed holes

Maximum bleed flow (percent of capture mass flow)

Cowl	14.28
Centerbody	7.82

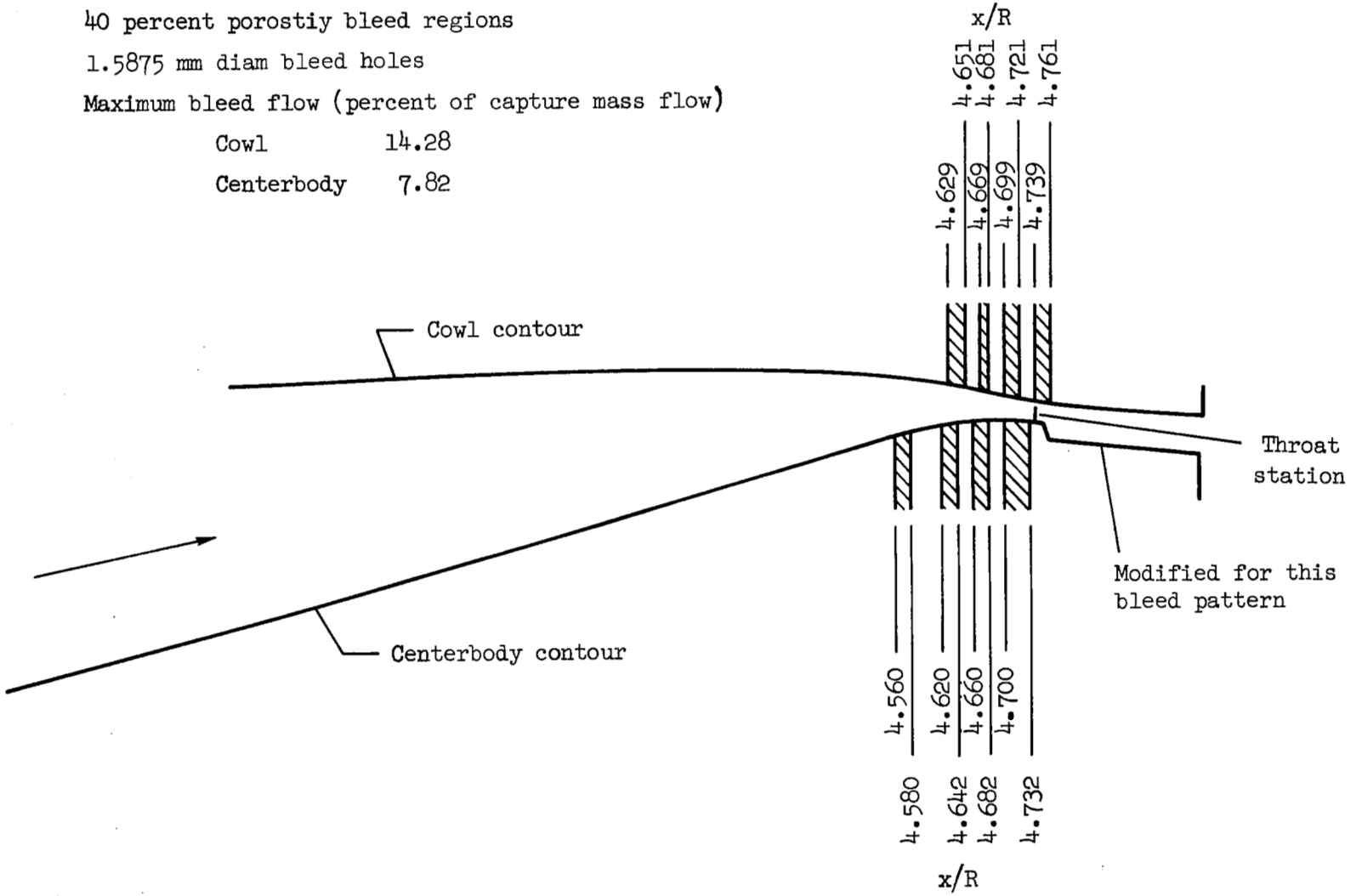

(b) Bleed pattern B

Figure 3.- Concluded.

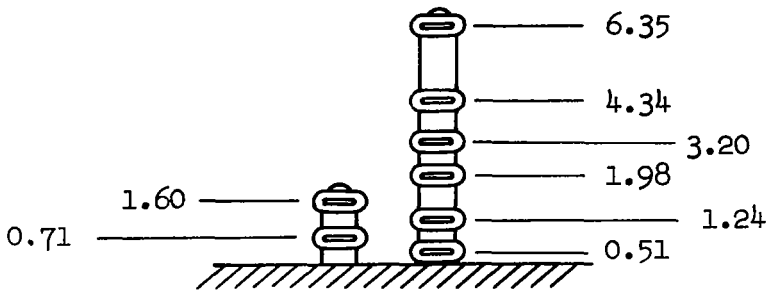

Boundary-layer rake

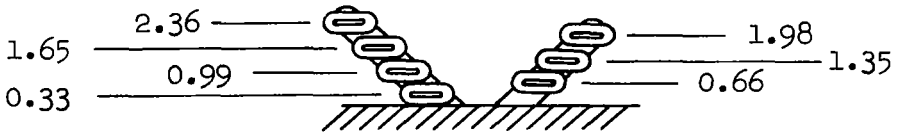

Throat rake No. 1

Note: All dimensions are the distance from the centerline of each aperture to the model surface in millimeters

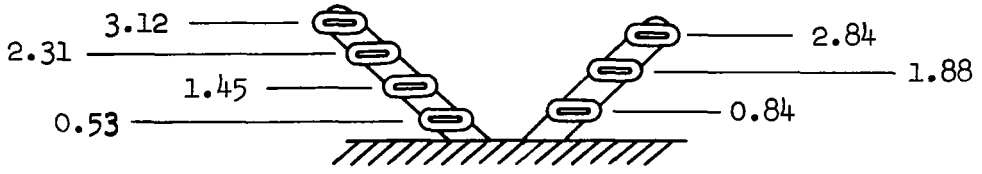

Throat rake No. 2

Figure 4.- Rake details.

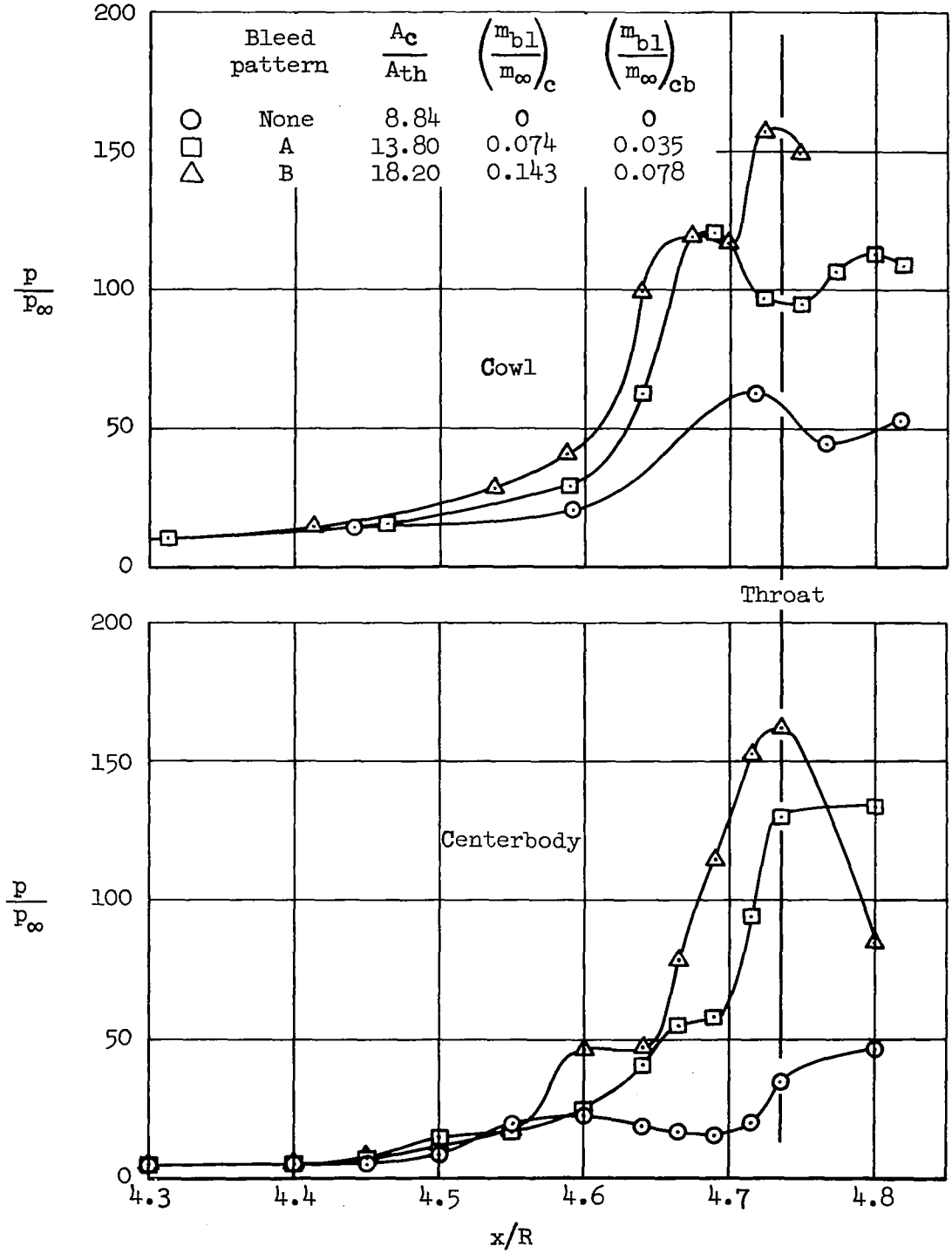

Figure 5.- Static-pressure distributions at maximum contraction ratio; $\alpha = 0°$.

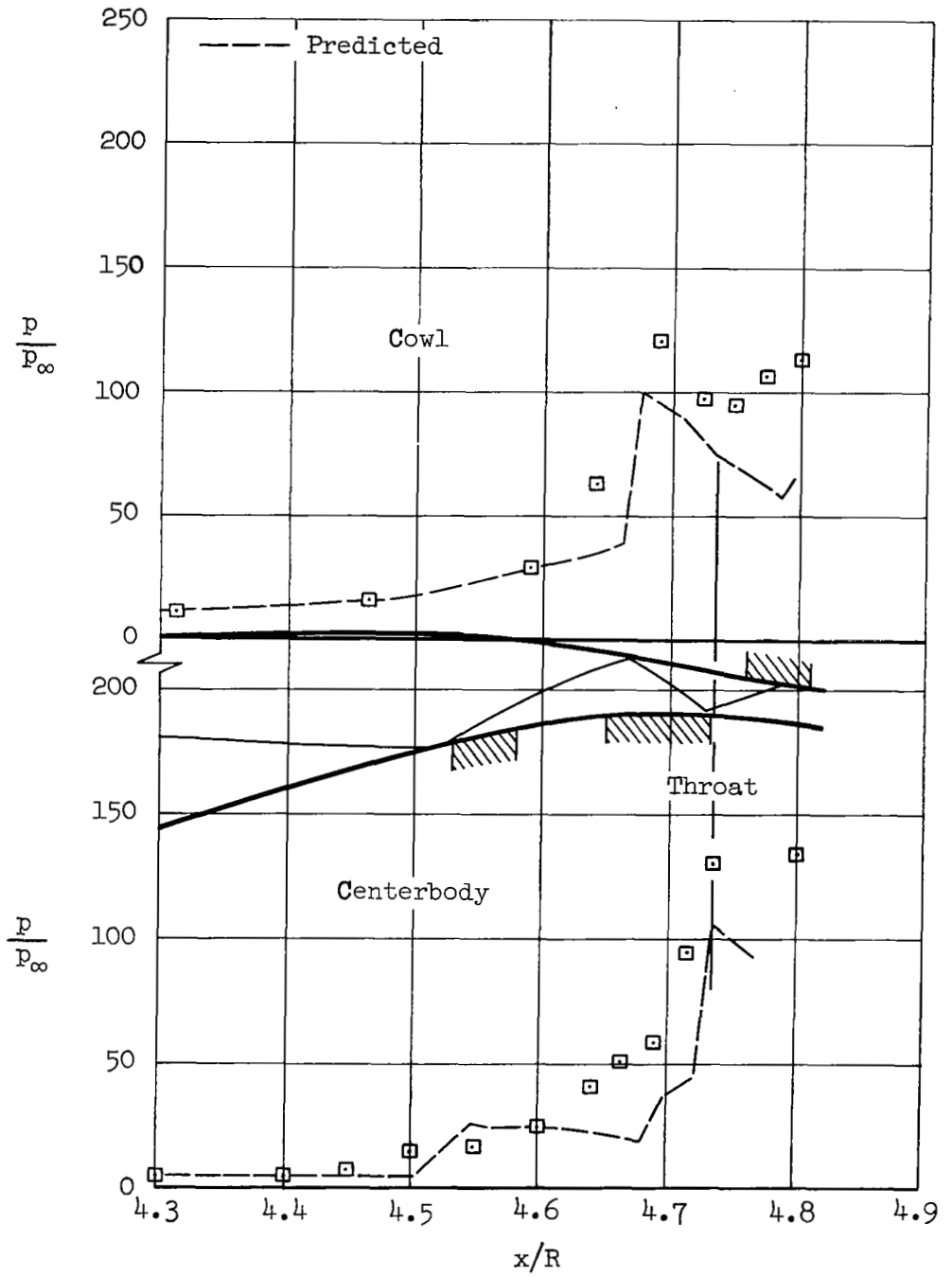

(a) Bleed pattern A, A_c/A_{th} = 13.8

Figure 6.- Comparison of data with theoretical static-pressure distributions; α = 0°.

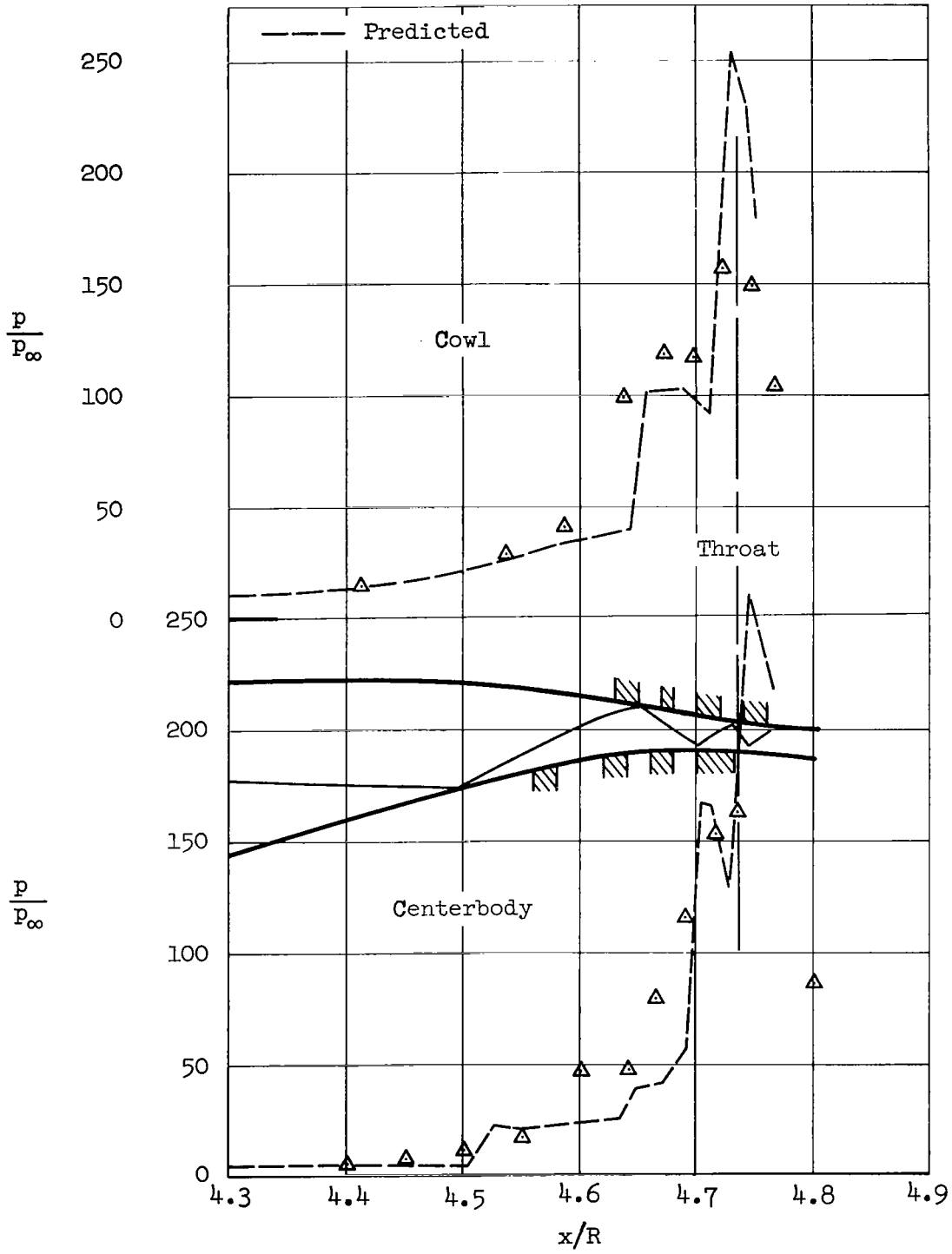

(b) Bleed pattern B, $A_c/A_{th} = 18.2$

Figure 6.- Concluded.

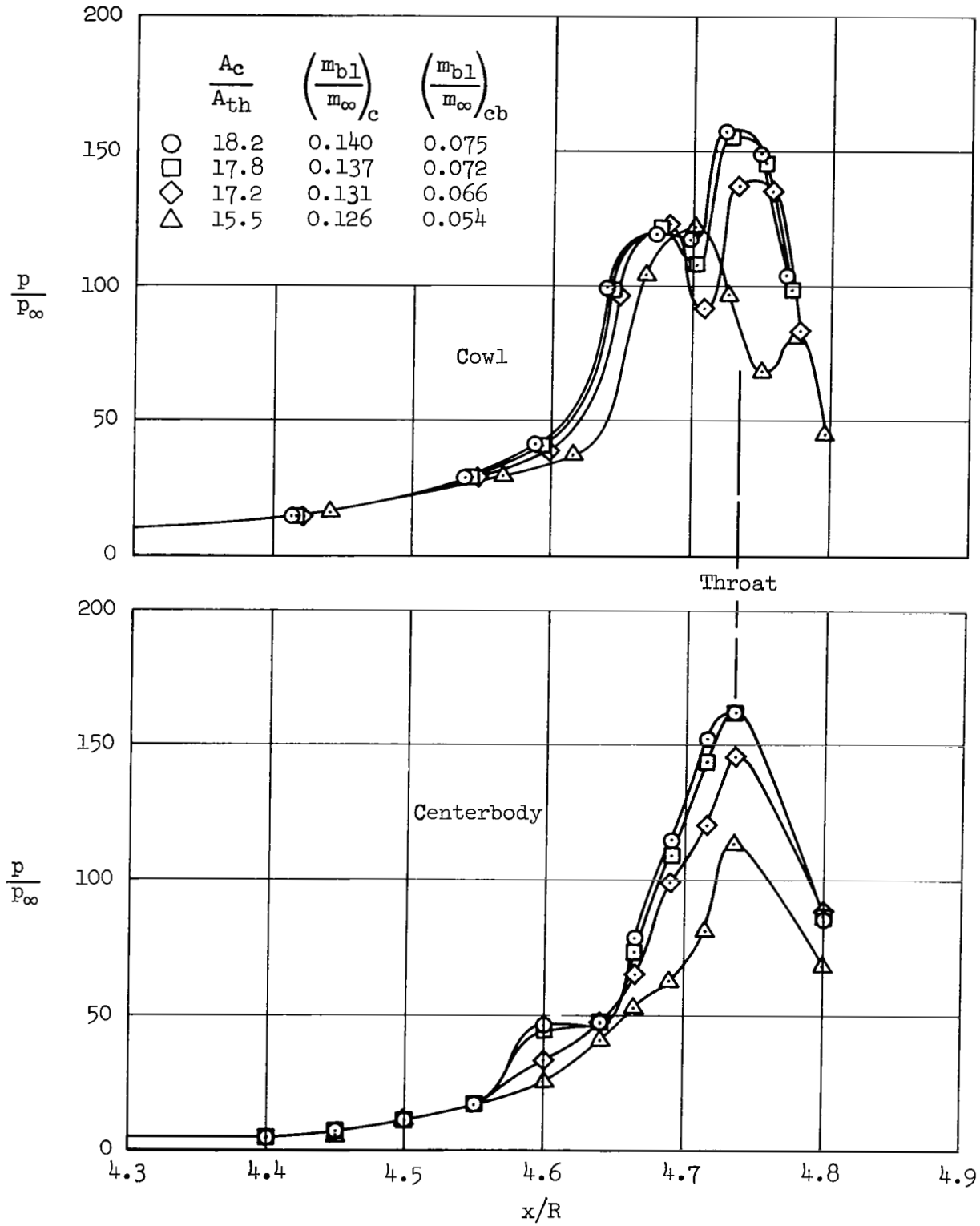

Figure 7.- Static-pressure distribution at various contraction ratios; bleed pattern B; $\alpha = 0°$.

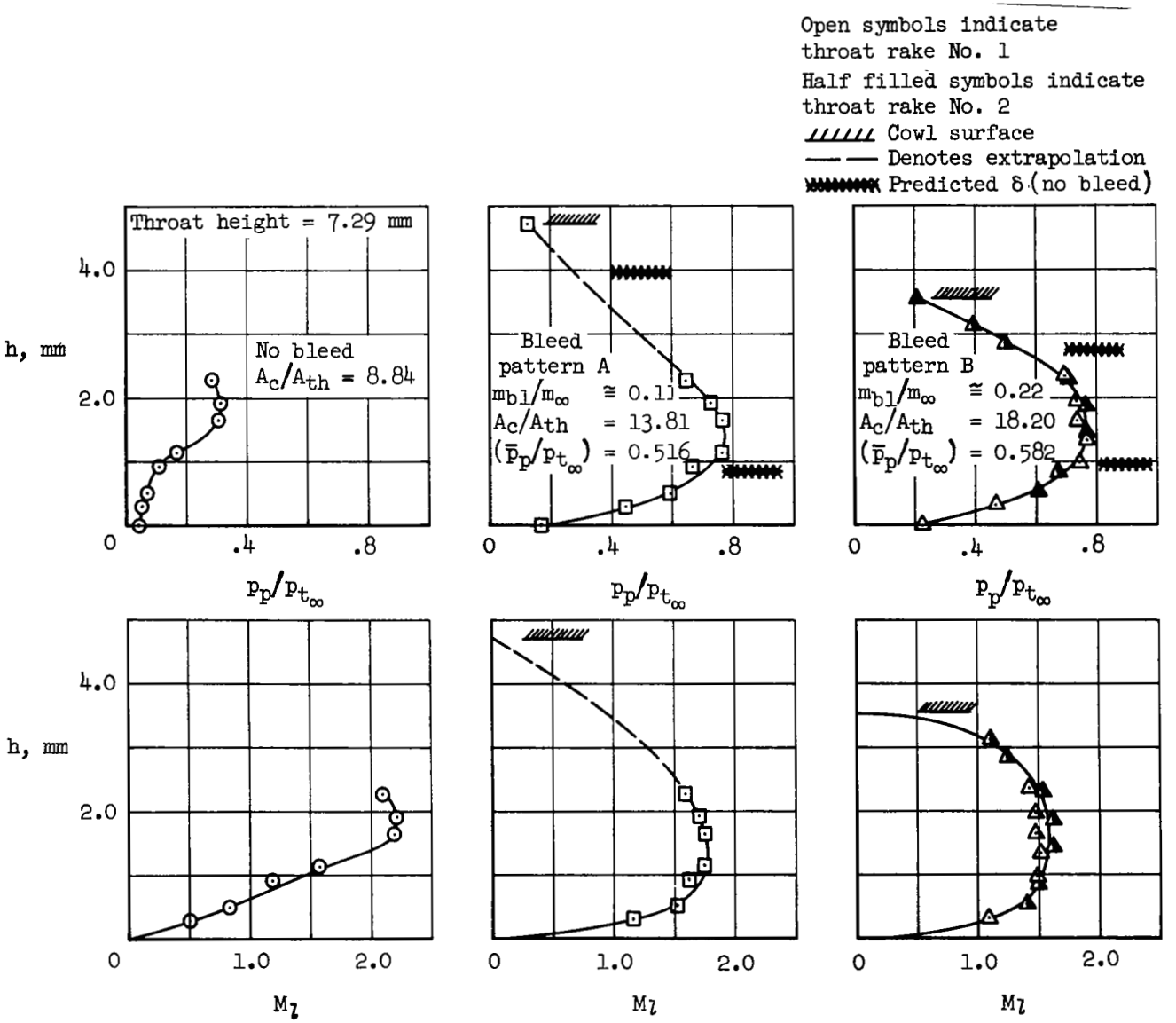

Figure 8.- Throat pitot pressure and Mach-number profiles; $\alpha = 0°$.

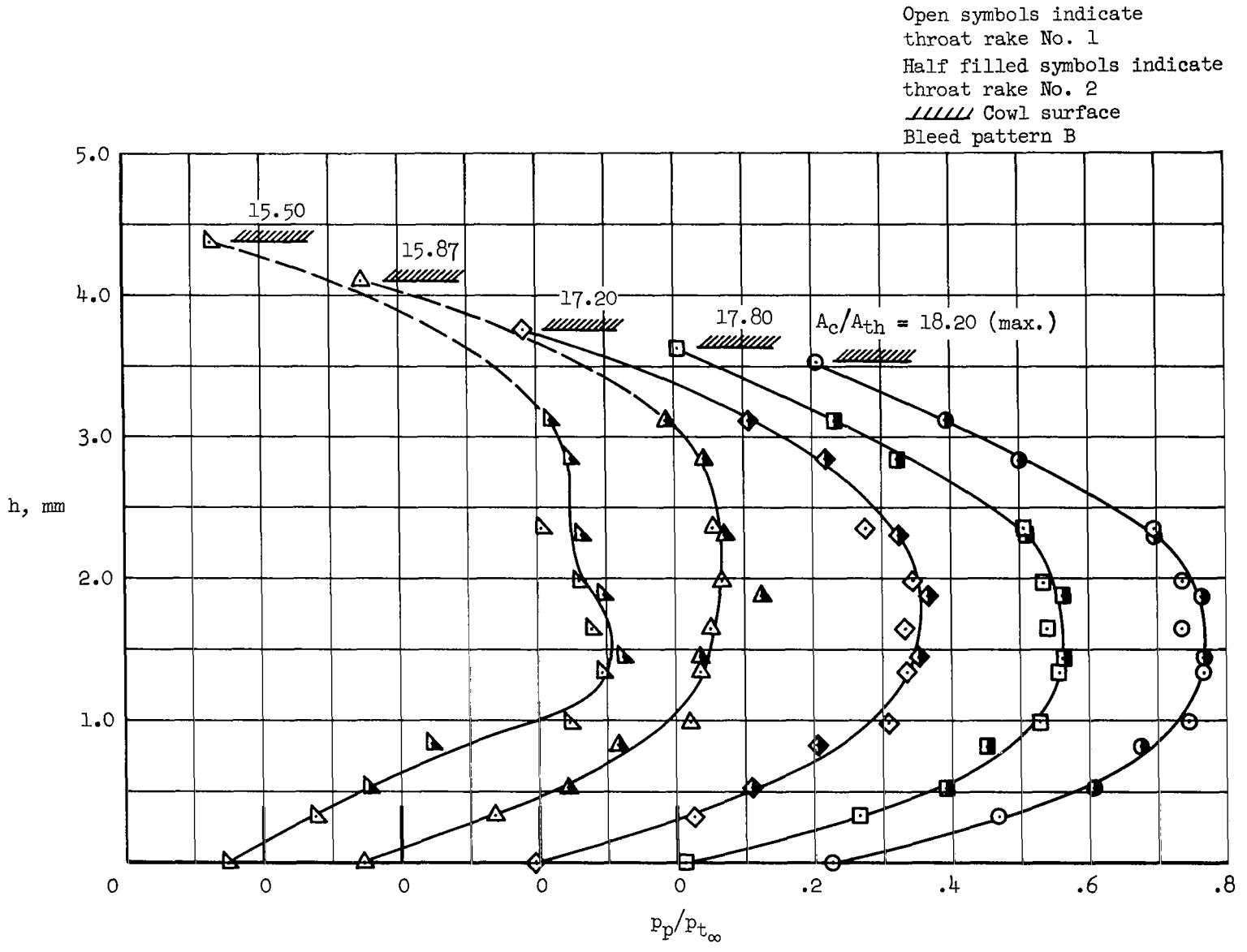

Figure 9.- Throat pitot pressure profiles at various contraction ratios; $\alpha = 0°$.

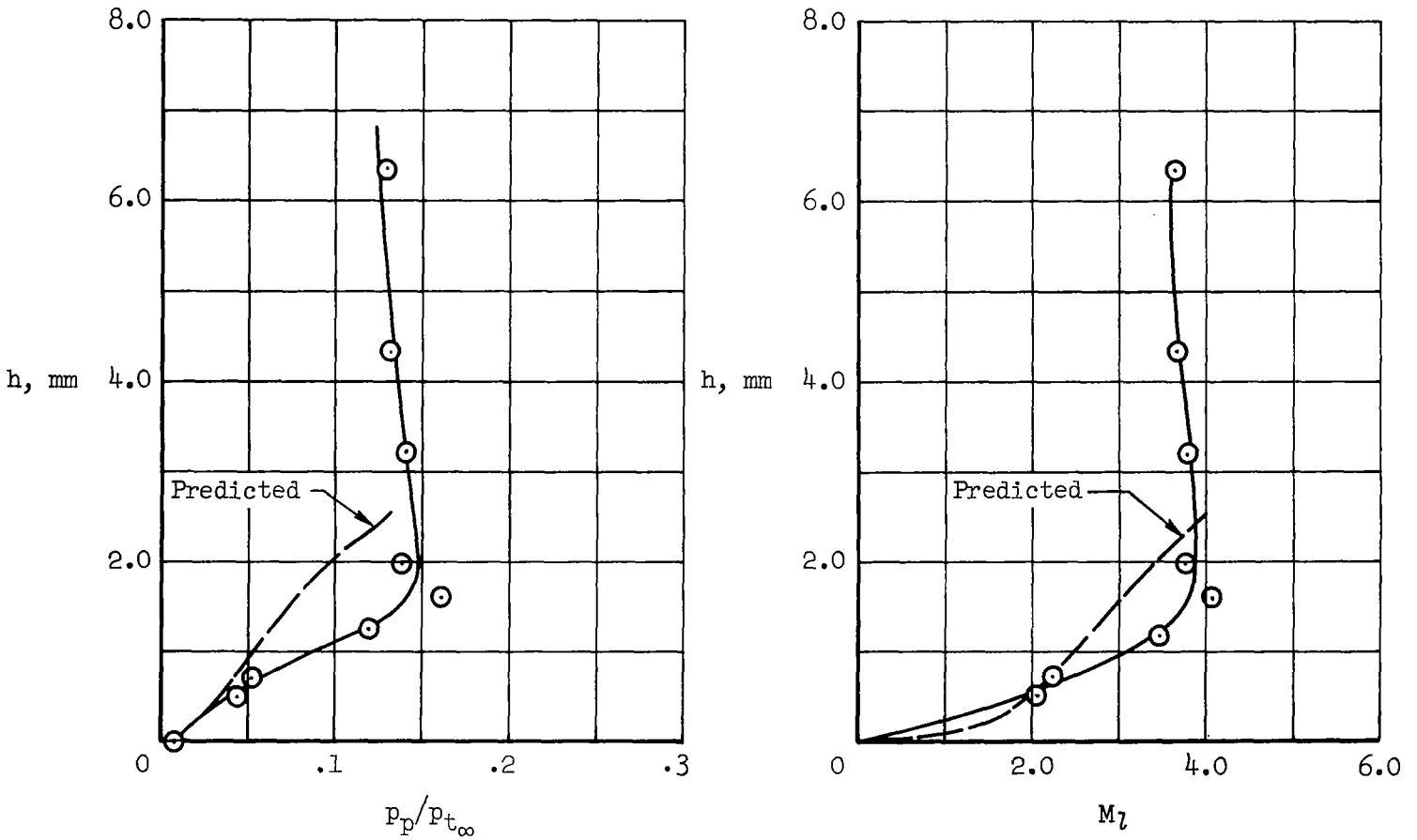

Figure 10.- Centerbody boundary-layer pitot pressure and Mach number profiles; x/R = 4.2, α = 0°.

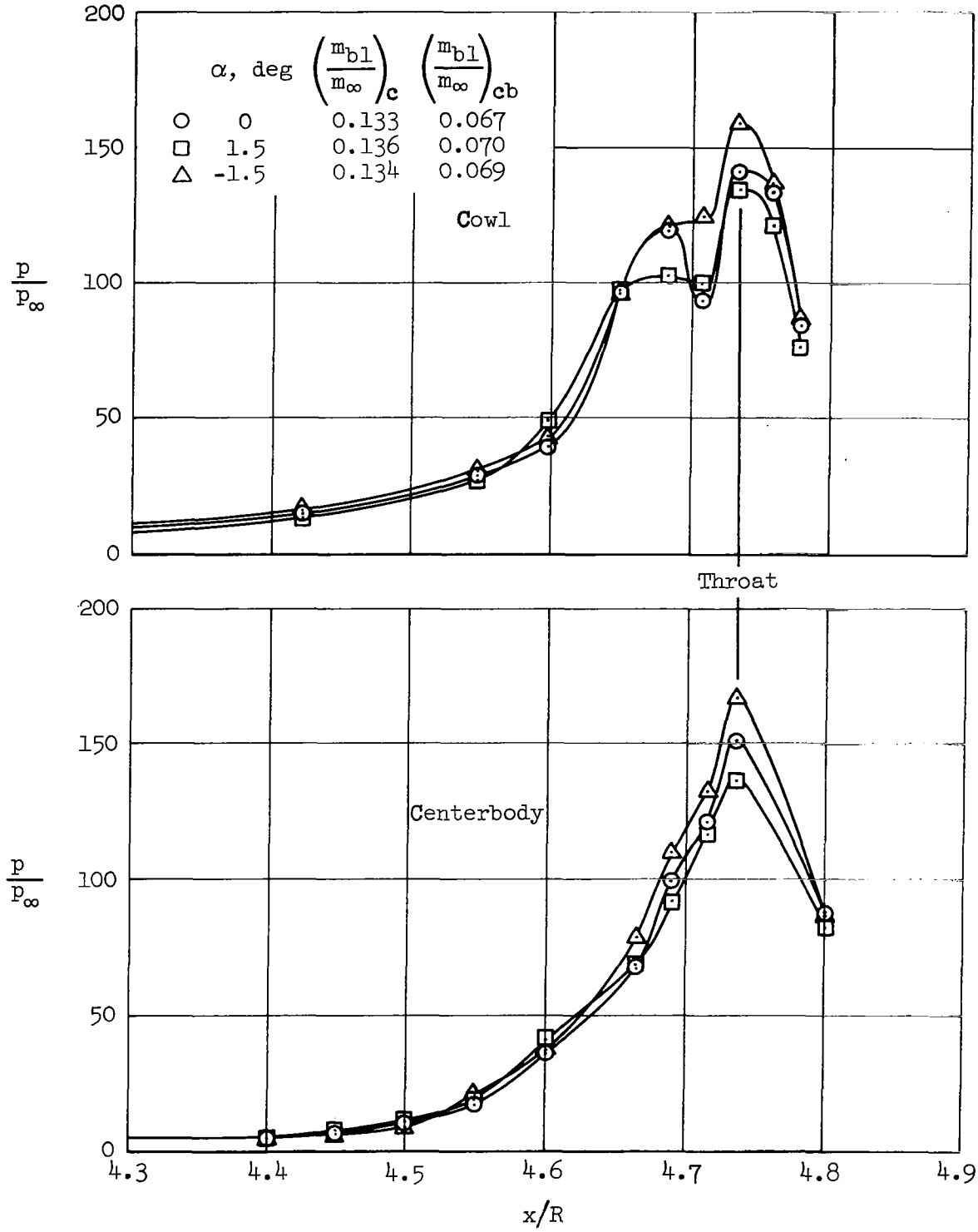

(a) $\alpha = \pm 1.5°$, $A_c/A_{th} = 17.2$

Figure 11.- Static-pressure distributions at angle of attack; bleed pattern B

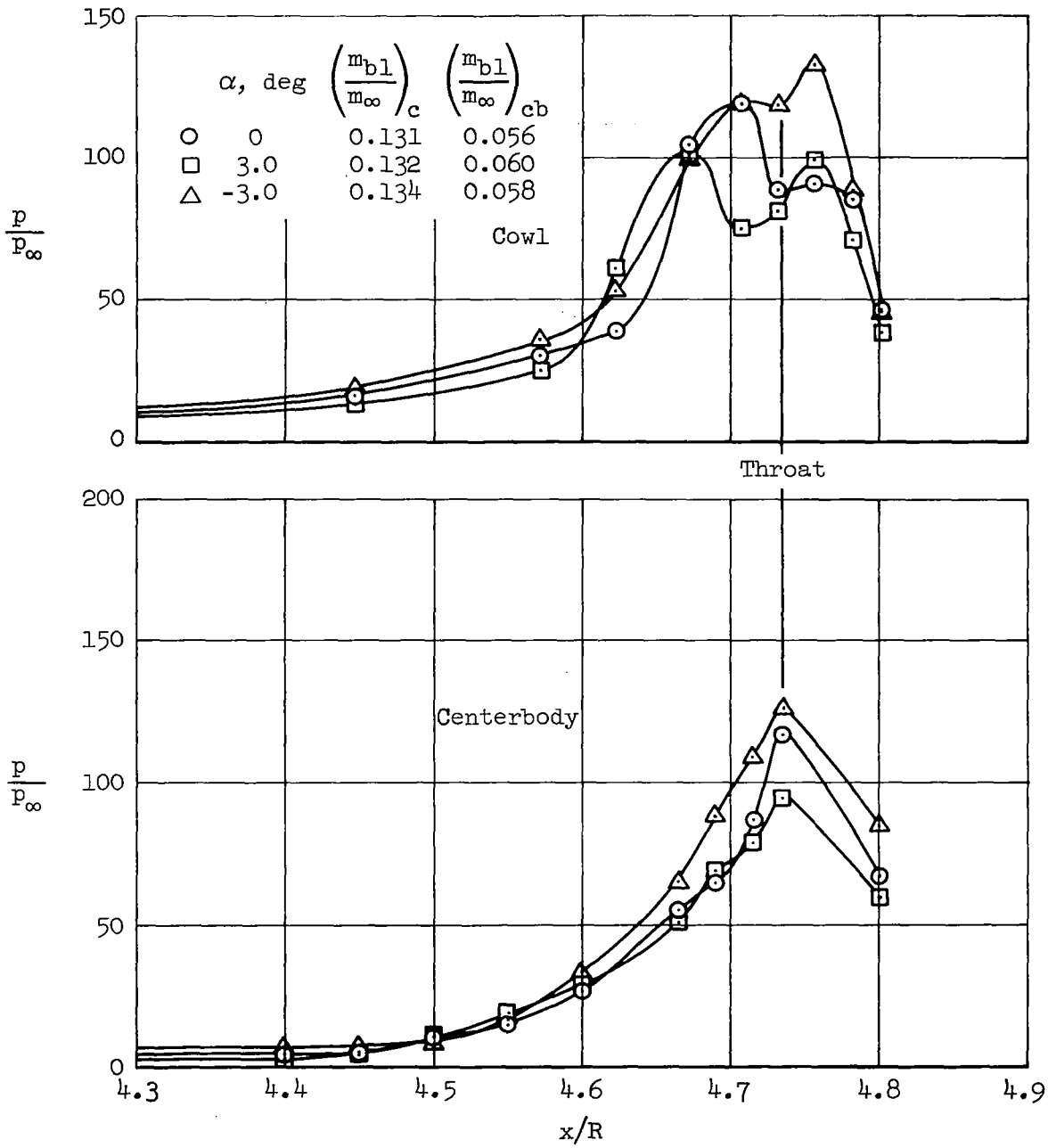

(b) $\alpha = \pm 3.0°$, $A_c/A_{th} = 15.1$

Figure 11.- Concluded.

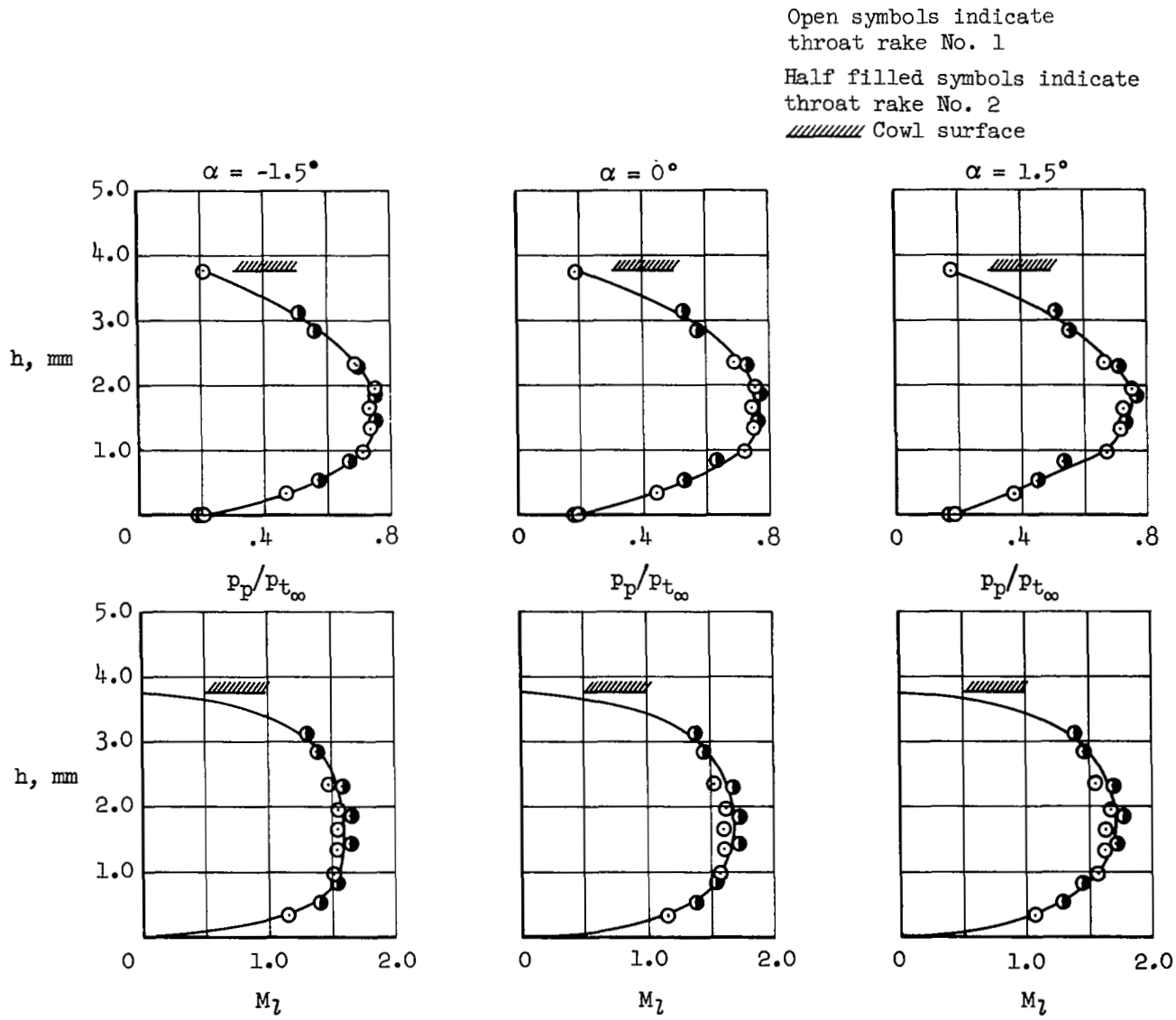

(a) $\alpha = \pm 1.5°$, $A_c/A_{th} = 17.2$

Figure 12.- Throat pitot pressure and Mach number profiles at angle of attack; bleed pattern B.

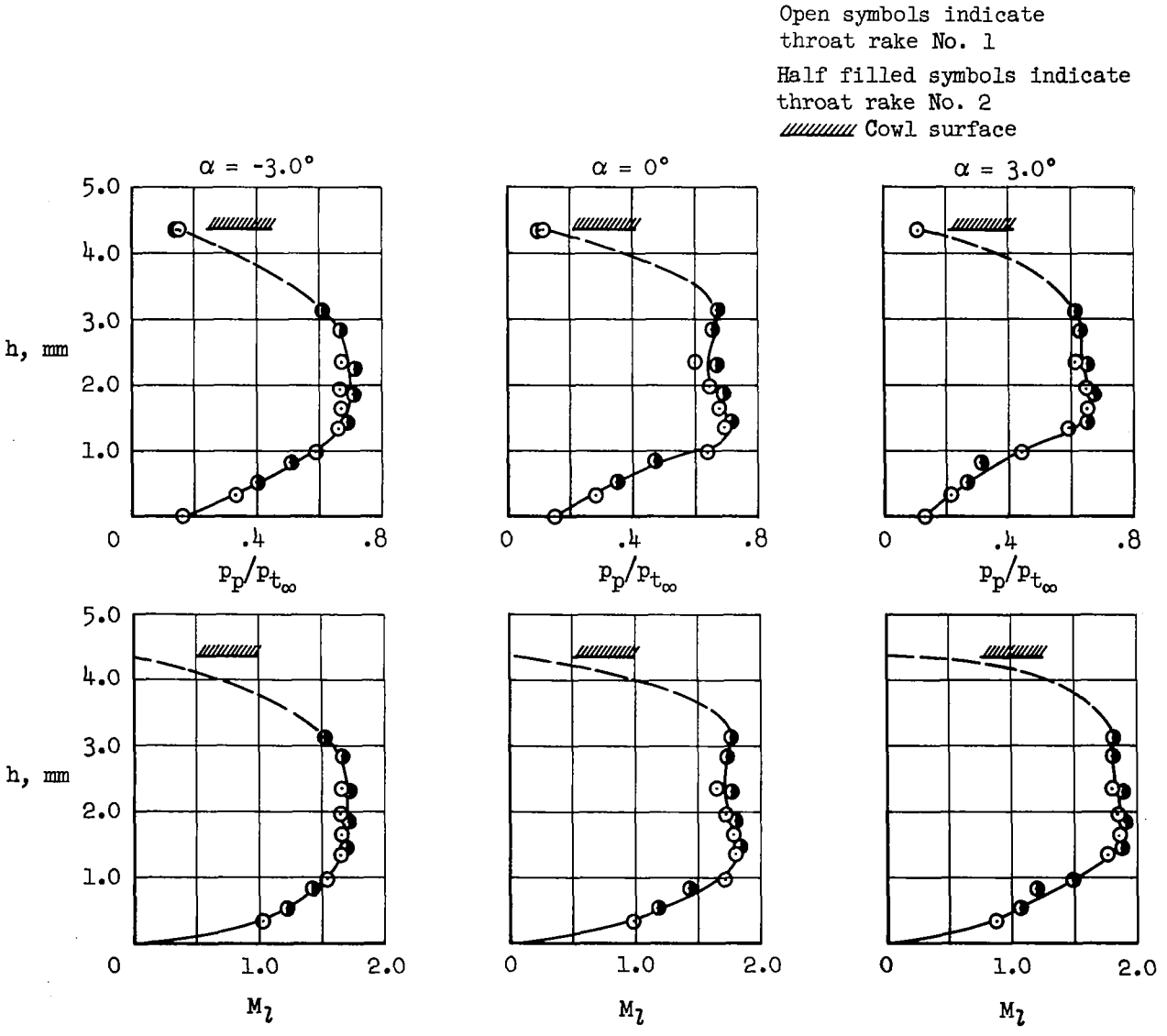

(b) $\alpha = \pm 3.0°$, $A_c/A_{th} = 15.1$

Figure 12.- Concluded.

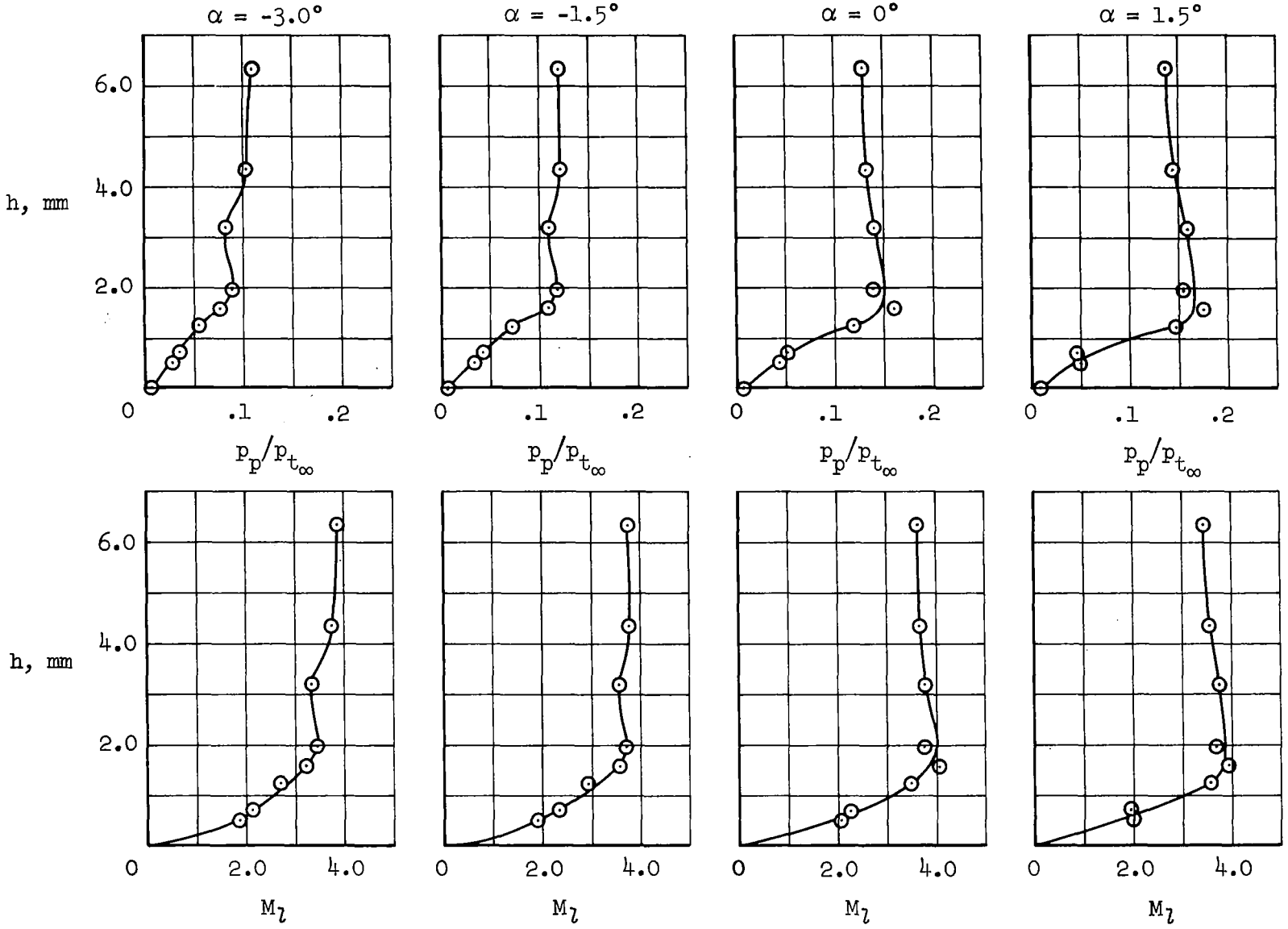

Figure 13.- Centerbody boundary-layer pitot pressure and Mach-number profiles at angle of attack; x/R = 4.2.

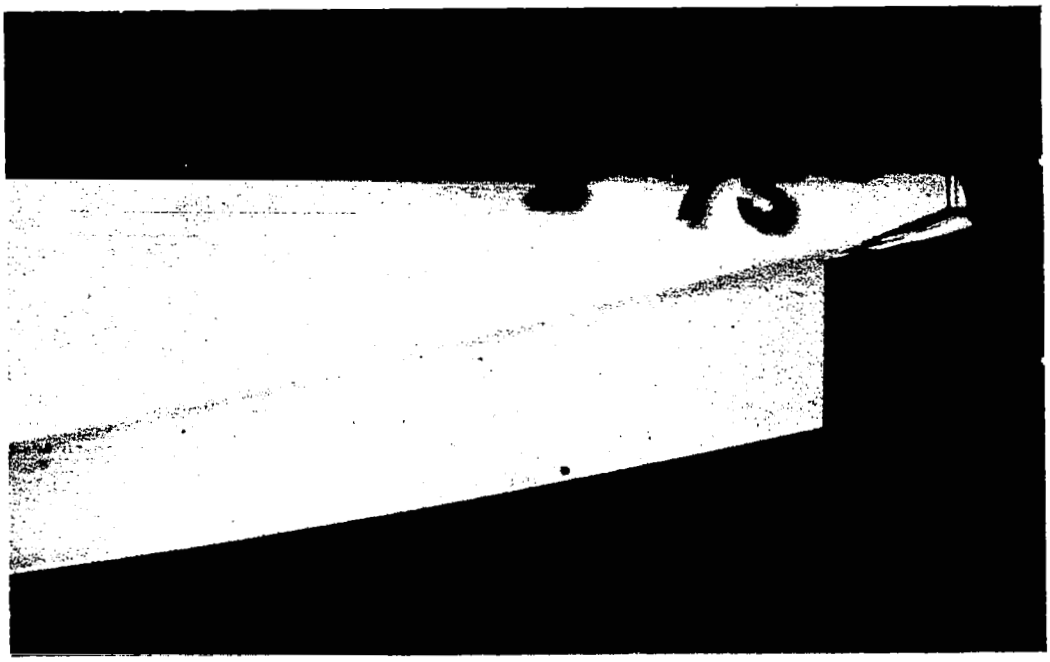

(a) $\alpha = 0°$

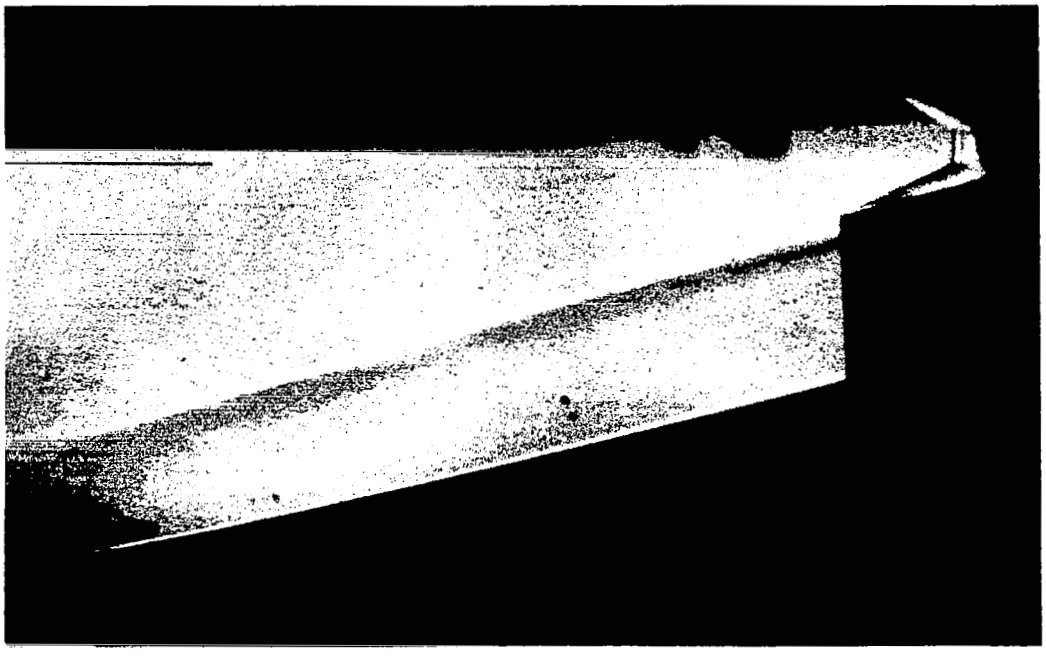

(b) $\alpha = -3.0°$

Figure 14.- Schlieren photographs.